Neurite outgrowth is driven by actin polymerization even in the presence of actin polymerization inhibitors

Jonathan X. Chia, Nadia Efimova, and Tatyana M. Svitkina*
Department of Biology, University of Pennsylvania, Philadelphia, PA 19104

ABSTRACT **Actin polymerization is a universal mechanism to drive plasma membrane protrusion in motile cells. One apparent exception to this rule is continuing or even accelerated outgrowth of neuronal processes in the presence of actin polymerization inhibitors. This fact, together with the key role of microtubule dynamics in neurite outgrowth, led to the concept that microtubules directly drive plasma membrane protrusion either in the course of polymerization or by motor-driven sliding. The possibility that unextinguished actin polymerization drives neurite outgrowth in the presence of actin drugs was not explored. We show that cultured hippocampal neurons treated with cytochalasin D or latrunculin B contained dense accumulations of branched actin filaments at ~50% of neurite tips at all tested drug concentrations (1–10 μM). Actin polymerization is required for neurite outgrowth because only low concentrations of either inhibitor increased the length and/or number of neurites, whereas high concentrations inhibited neurite outgrowth. Of importance, neurites undergoing active elongation invariably contained a bright F-actin patch at the tip, whereas actin-depleted neurites never elongated, even though they still contained dynamic microtubules. Stabilization of microtubules by Taxol treatment did not stop elongation of cytochalasin–treated neurites. We conclude that actin polymerization is indispensable for neurite elongation.**

Monitoring Editor
Laurent Blanchoin
CEA Grenoble

Received: Apr 25, 2016
Revised: Sep 19, 2016
Accepted: Sep 20, 2016

INTRODUCTION

Cell migration and cell shape changes play vital roles in normal physiology and pathology of multicellular organisms by contributing to development, morphogenesis, immunity, wound healing, and cancer. Cell motility is driven by activity of the cytoskeleton with actin filaments and microtubules being the key players in this process. Actin polymerization in the form of branched networks in lamellipodia and parallel bundles in filopodia is the major mechanism to drive leading-edge protrusion in motile cells (Svitkina, 2013). Assembly of branched actin filament networks involves activity of the Arp2/3 complex (Svitkina *et al.*, 1997; Svitkina and Borisy, 1999; Mullins *et al.*, 1998), which nucleates new actin branches on the side of preexisting actin filaments (Mullins *et al.*, 1998). Formation of filopodial actin bundles depends on the elongation-promoting activity of formins and Ena/VASP family proteins and actin cross-linking proteins that mediate bundling (Svitkina, 2013).

In most cell types, directional cell migration requires the contribution of microtubules. After disruption of microtubules in fibroblasts, the actin cytoskeleton retains its ability to produce protrusion and contraction, but these activities are disorganized, and cells fail to translocate (Vasiliev *et al.*, 1970). Similarly, disruption of microtubules in neurons caused outgrowing neurites to stop or collapse (Yamada *et al.*, 1970). Not only integrity, but also the dynamic status of microtubules is important, although dynamic microtubules are required in some cases (Tanaka *et al.*, 1995; Dent and Kalil, 2001; Kaverina *et al.*, 2002; Rajnicek *et al.*, 2006), whereas stable microtubules are sufficient or even beneficial in other situations (Gundersen and Bulinski, 1988; Buck and Zheng, 2002; Witte *et al.*, 2008; Lu *et al.*, 2013). Several nonexclusive mechanisms of microtubule-dependent regulation of actin dynamics have been considered: 1) delivery of "protrusion-promoting" factors to the cell front by stable microtubules (Gundersen and Bulinski, 1988); 2) regulation of Rho

This article was published online ahead of print in MBoC in Press (http://www.molbiolcell.org/cgi/doi/10.1091/mbc.E16-04-0253) on September 28, 2016.
*Address correspondence to: Tatyana Svitkina (svitkina@sas.upenn.edu).
Abbreviations used: CytoD, cytochalasin D; DIV, days in vitro; LatB, latrunculin B; PREM, platinum replica electron microscopy.

GTPases to stimulate Rac-dependent protrusion at the front and Rho-dependent retraction at the rear, depending on the total amount of microtubules (Waterman-Storer *et al.*, 1999; Krendel *et al.*, 2002; Siegrist and Doe, 2007); and 3) targeting of cell–matrix adhesions by dynamic microtubules to cause their disassembly, preferentially at the rear (Kaverina *et al.*, 2002).

A more direct role of microtubules in cell motility has been proposed based on studies of neuron development in culture. Microtubules are the main cytoskeletal components of neurites. They support the structural integrity of neuronal processes and mediate long-distance traffic along neurite shafts. However, extension and navigation of neurites are normally driven by actin-rich growth cones positioned at the neurite tips (Dent *et al.*, 2011; Bradke *et al.*, 2012; Gallo, 2013). Most microtubules entering the growth cone from the neurite shaft terminate at a distance from the cell plasma membrane, whereas actin filaments in lamellipodia and filopodia are positioned at the forefront of the growth cone and abut the plasma membrane (Bridgman *et al.*, 1986; Forscher and Smith, 1988), as expected for the actin polymerization–driven protrusion. However, in the presence of actin polymerization inhibitors, neurite extension continues or even is enhanced (Letourneau *et al.*, 1987; Bradke and Dotti, 1999; Ruthel and Hollenbeck, 2000; Dent and Kalil, 2001; Flynn *et al.*, 2012; Lu *et al.*, 2013). These observations led to the concept that microtubules directly drive membrane protrusion by pressing onto the plasma membrane either in the course of polymerization or via motor-driven sliding, whereas actin cytoskeleton inhibits neurite elongation by blocking access of microtubules to the membrane (Letourneau *et al.*, 1987; Lu *et al.*, 2013). Moreover, this mechanism is also considered to have universal significance and be applicable to other cell types (Etienne-Manneville, 2013).

Although the idea of microtubules directly driving protrusion is consistent with observations, it conflicts with the classic concept that actin polymerization drives membrane protrusion in all other systems except blebs that are inflated by intracellular pressure (Paluch and Raz, 2013). Therefore additional evidence is needed to test the unconventional possibility that microtubules directly drive protrusion, especially because most reports on the proposed microtubule-driven protrusion did not provide evidence that actin filaments were fully depolymerized in drug-treated neurons. When such evidence was provided (Lu *et al.*, 2013), the absence of F-actin at the neurite tips specifically during the extension phase was not demonstrated. Here, we show that neurite elongation in the presence of actin-depolymerizing drugs is invariably driven by unextinguished actin polymerization. Therefore actin polymerization can maintain its status as a universal mechanism to drive plasma membrane protrusion, whereas potential mechanisms by which microtubules influence cell migration can be narrowed to those by which microtubules regulate the actin cytoskeleton.

RESULTS AND DISCUSSION

To determine whether actin filaments are dispensable during neurite extension in the presence of actin-depolymerizing drugs, we cultured rat hippocampal neurons in the presence of cytochalasin D (CytoD) and latrunculin B (LatB), which interfere with actin polymerization using different mechanisms: CytoD caps barbed ends of actin filaments, whereas LatB sequesters actin monomers. It was previously observed that relatively low concentrations of these or closely related (cytochalasin B and latrunculin A) drugs do not prevent and might even enhance neurite outgrowth in different types of neurons (Letourneau *et al.*, 1987; Bradke and Dotti, 1999; Flynn *et al.*, 2012; Lu *et al.*, 2013), leading to the idea that actin polymerization is not required for neurite extension.

Neurite outgrowth is promoted by low but not high concentrations of LatB or CytoD

Neurons were cultured for 48 h after plating in a normal medium and then treated for an additional 24 h with a range of LatB or CytoD concentrations, as well as with dimethyl sulfoxide (DMSO) as control. Fixed cultures were stained with phalloidin to reveal F-actin and with Tuj1 antibody to a neuron-specific β3 isoform of tubulin to reveal microtubules and identify neurons (Figure 1). The results showed that many untreated and DMSO-treated neurons were polarized at this time, as expected based on the well-characterized developmental program of hippocampal neurons in tissue culture (Banker and Cowan, 1977). Polarized neurons formed several microtubule-rich neurites tipped with F-actin–rich growth cones having clearly recognizable filopodia and lamellipodia (Figure 1, A and B). Some cells in these cultures remained unpolarized and formed broad actin-rich protrusions around most of their periphery.

In the presence of 1–10 μM LatB or CytoD, neurons exhibited multiple neurite-like processes. Remarkably, about half of these neurites contained a bright F-actin structure at the tip even at the highest tested drug concentration (Figure 1C). In contrast to normal growth cones, F-actin accumulations at the neurite tips in drug-treated neurons were small, had a compact, bulb-like shape, and lacked obvious filopodia (Figure 1B). In addition to the actin bulbs at neurite tips, fainter F-actin accumulations could be observed along the neurite shafts, especially at low inhibitor concentrations and more often in CytoD-treated neurons. In addition, small F-actin speckles occasionally outlined some cell margins in drug-treated neurons (Figure 1B), probably where broad lamellae existed before inhibitor application. However, all types of F-actin accumulations became progressively dimmer and smaller as the LatB or CytoD concentration was increased. Thus, even at the highest tested concentration, neither LatB nor CytoD eliminates F-actin in neurons. Moreover, the remaining F-actin preferentially localizes at the neurite tips. This preference could potentially result from abundance of microtubule ends at these sites, if microtubules deliver some signals that would trigger actin assembly, or from microtubule stabilization at the neurite tips, as suggested by existing models of actin–microtubule cross-talk (Gundersen and Bulinski, 1988; Waterman-Storer *et al.*, 1999; Etienne-Manneville, 2013). In any case, drug-resistant actin filaments at the neurite tips are properly positioned to maintain sustained neurite outgrowth in the presence of CytoD or LatB.

If actin polymerization is required to support neurite elongation, then it should be increasingly difficult for neurons to extend neurites as the LatB or CytoD concentration is increased. Therefore we evaluated the dose-dependent effects of LatB and CytoD on neurite outgrowth by measuring an average length of the longest neurite and an average number of neurite-like processes per neuron in different conditions (Figure 1, D and E). Different quantification criteria, such as total or average neurite length per neuron or an average length of all neurites in the population, yielded similar results. After treatment with 1 μM LatB, both the average length of the longest neurite and the number of neurites per cell were increased compared with DMSO-treated cultures, whereas only the average number of processes was increased after treatment with 1 μM CytoD. However, treatment with the high LatB concentration (10 μM) significantly reduced both parameters below the control levels, whereas treatment with 10 μM CytoD reduced the average number of processes per cell to the control value (Figure 1, D and E). Less dramatic effects of CytoD compared with LatB are consistent with the lower potency of CytoD in causing actin depolymerization. However, morphology of neurites in cultures treated with 10 μM CytoD was highly abnormal, with broad and poorly shaped cell processes (Figure 1B).

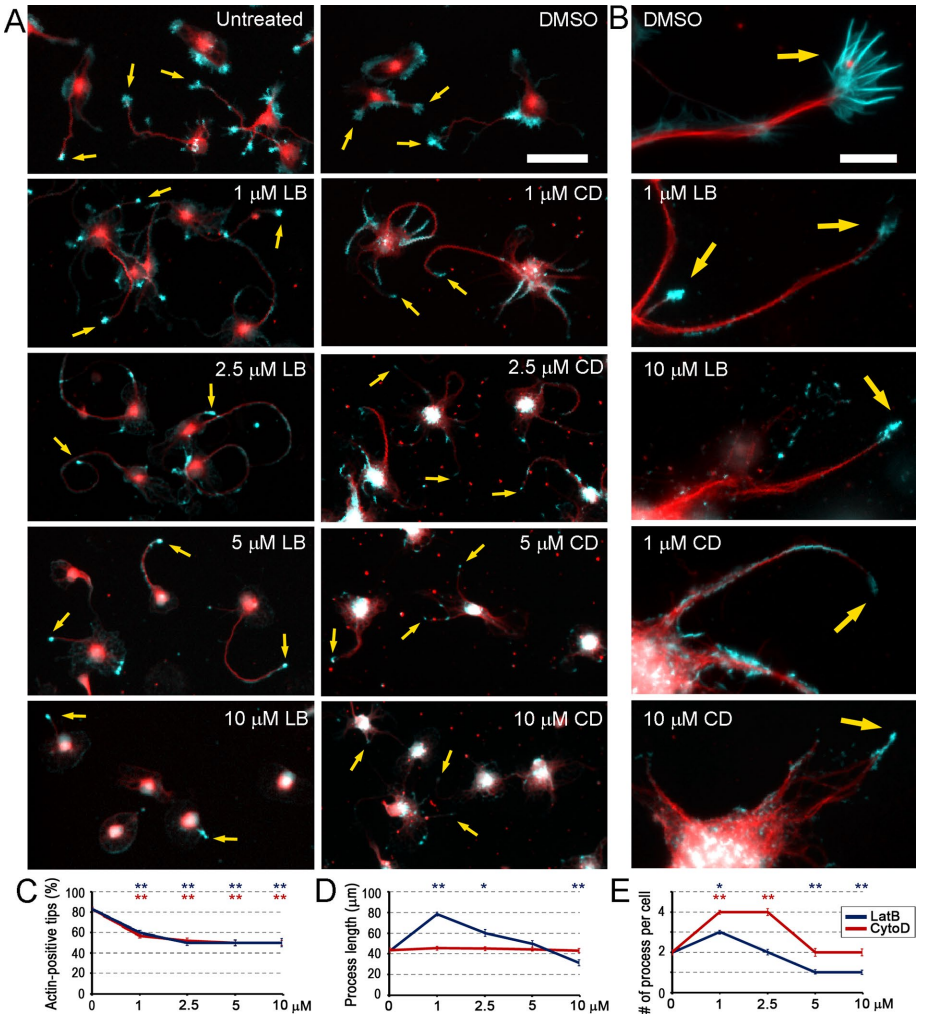

FIGURE 1: Dose-dependent effects of LatB and CytoD on neurite outgrowth and accumulation of F-actin at neurite tips. (A, B) Rat hippocampal neurons cultured for 3 DIV in normal medium (untreated) or treated with DMSO or indicated concentrations of LatB (LB) or CytoD (CD) during the last 24 h. Fixed cells were stained with phalloidin (cyan) or Tuj1 antibody (red). Arrows point to F-actin accumulations. Scale bars, 50 μm (A), 10 μm (B). (C–E) Concentration dependence of the average percentage of F-actin–positive neurite tips (C; 98–407 neurites), average length of the longest neurite (D; 96–338 neurites), and average number of neurites per cell (E; 172–472 neurites) in neuron cultures treated with LatB (blue) or CytoD (red). Median ± SEM. Statistical significance (*$p < 0.01$; **$p < 0.001$) determined relative to DMSO treatment.

Of note, there was also a significant loss of adherent cells in cultures treated with high LatB or CytoD concentrations, as evident from considerably decreased cell densities and the presence of "cell ghosts" on the substrate (faint fluorescence signals shaped as a cell without the actual cell present). Therefore the quantitative results likely underestimate the magnitude of deterioration of cell spreading caused by high concentrations of LatB or CytoD.

The ability of actin-depolymerizing drugs to inhibit neurite outgrowth when actin assembly is efficiently suppressed supports the idea that actin polymerization is necessary for neurite extension. Then why do low doses of LatB or CytoD enhance neurite outgrowth? The actin cytoskeleton has two major functions in cell motility, including motility of growth cones—actin polymerization pushes the growth cone forward, whereas actin–myosin contraction pulls it backward. If low drug concentrations have a greater effect on the contractile system than on protrusive machinery, the overall balance of forces in the growth cone would favor protrusion and promote neurite elongation. Indeed, we reported previously that branched actin networks that generate pushing forces are better able to withstand the LatB treatment and are last to be destroyed by the drug compared with contractile actin–myosin structures (Svitkina and Borisy, 1999; Collins *et al.*, 2011). However, at high doses of actin-depolymerizing drugs, the protrusive activity of the actin cytoskeleton also begins to deteriorate, and neurite outgrowth is impaired. Different drug concentrations may also have differential effects on cell adhesion, which also depends on actin cytoskeleton.

Actin bulbs remaining at neurite tips after LatB or CytoD treatment consist of dense branched actin networks

A conspicuous localization of F-actin bulbs surviving the LatB or CytoD treatment at the neurite tips suggests that these bulbs may be protrusive organelles driving neurite outgrowth. Alternatively, they may represent nonfunctional aggregates of actin filaments. We used platinum replica electron microscopy (PREM) to determine the high-resolution structure of actin bulbs at the tips of drug-treated neurons and thus reveal whether this structure is consistent with the role of bulbs in membrane protrusion.

PREM showed that growth cones of control neurons cultured for 3 d in vitro (DIV3) in a normal medium contained a mixture of actin filament bundles in filopodia and branched actin filament networks in lamellipodia (Figure 2A), as reported previously (Korobova and Svitkina, 2008). PREM analysis of neurons treated with 2.5 μM LatB (Figure 2B) or 2.5 μM CytoD (Figure 2C) demonstrated that actin bulbs at the neurite tips contained dense networks of branched actin filaments composed of short actin filaments with numerous filament ends. Although network densities varied broadly, many actin bulbs at the neurite tips were very dense. We found no obvious actin filament bundles in drug-treated neurons.

The main (or even only) known function of branched actin filament networks in cells is to generate pushing force. Therefore the existence of branched actin networks at the neurite tips strongly suggests that Arp2/3 complex–dependent actin polymerization is chiefly responsible for neurite extension in the presence of CytoD or LatB. Indeed, branched organization of these actin structures poorly correlates with the idea that they are nondepolymerizable actin aggregates because branched actin networks are typically highly dynamic and quickly disassemble in cells if their depolymerization is not balanced by polymerization. Of note, CytoD-resistant actin filaments were also observed by others at plasma membrane sites that are normally occupied by branched actin networks (Forscher and Smith, 1988; Zhang *et al.*, 2016). Although these actin structures were interpreted as stable, their structure or dynamics were not investigated, leaving the question open. It is also hardly possible that actin filament

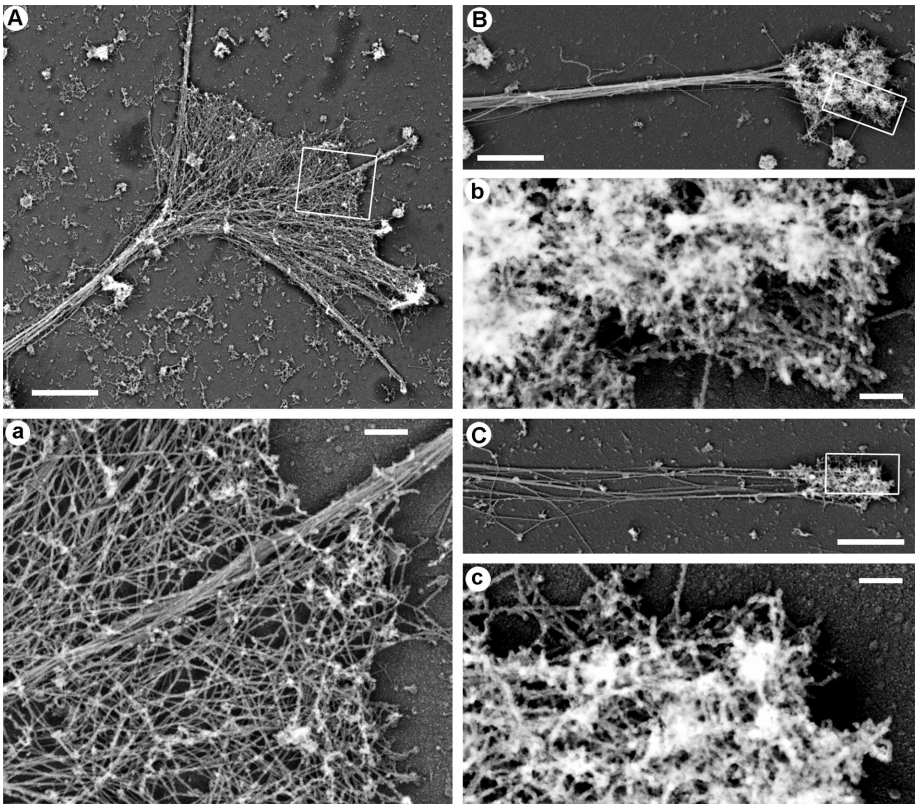

FIGURE 2: PREM of cytoskeleton structure in distal neurite regions. (A) Growth cone and a distal portion of the neurite from a neuron cultured in a normal medium. (a) Boxed region in A enlarged to show actin filament bundle in the filopodium and branched actin network in lamellipodia. (B, C) Actin-rich bulbs and the distal neurite regions from neuron treated with 2.5 μM LatB (B) or 2.5 μM CytoD (C). (b, c) Boxed regions in B and C, respectively, enlarged to show dense branched actin network in the actin bulb. Scale bars, 2 μm (A–C), 200 nm (a–c).

branches were formed by annealing (Andrianantoandro *et al.*, 2001) because annealing is expected to produce long, unbranched filaments. In the case of CytoD, which caps barbed ends (Bonder and Mooseker, 1986), one can imagine that actin filaments elongate from the pointed ends. However, this idea is also inconsistent with actin filament branching because pointed ends in the dendritic actin network are capped by the Arp2/3 complex. Therefore subsistence of branched actin filaments at the neurite tips in the presence of LatB or CytoD is most likely explained by incomplete inhibition of actin polymerization by these drugs. Because LatB and CytoD have finite association and dissociation rates for interaction with actin, some free actin monomers (for LatB) and uncapped barbed ends (for CytoD) are expected to be present even at high drug concentrations and support a limited level of actin polymerization. If sharply focused at the neurite tips, as appears to be the case, these limited levels of actin polymerization can be sufficient to drive neurite protrusion.

Neurites elongating in the presence of LatB or CytoD invariably contain an actin bulb at their tips

Both actin-positive and actin-negative neurite tips were found in fixed neuronal cultures treated with different concentrations of LatB or CytoD. Therefore it was possible that actin-negative neurites elongated in an actin-independent manner and their extension was driven by microtubules. Alternatively, actin-negative neurites could have elongated in an actin-dependent manner but stopped and lost actin by the time of fixation. To distinguish these possibilities, we used two live-cell imaging approaches.

In one approach (Figure 3), we transfected neurons with an F-actin reporter, F-tractin–tdTomato (Johnson and Schell, 2009), and treated them with either 1 μM LatB (Figure 3, A–D, and Supplemental Video S1) or 1 μM CytoD (Figure 3, E–H, and Supplemental Video S2). Neurons were imaged by time-lapse fluorescence microscopy to observe F-actin dynamics and by phase contrast microscopy to monitor neurite behavior. We found that all neurites that elongated in the presence of LatB or CytoD invariably contained a prominent F-tractin signal at their tips (Figure 3, A–D, tips 1–3, and E–H, tips 1 and 2). These F-tractin–positive neurite tips constantly changed their shapes during migration, suggesting that actin filaments within these regions were dynamic (Supplemental Videos S1 and S2). Some F-tractin–positive neurite tips remained stationary (Figure 3, E–H, tip 3) but exhibited prominent dynamic behavior without net translocation (Figure 3J). In fact, even F-tractin–positive bulbs that barely changed their shapes were not completely static but exhibited subtle morphing (Supplemental Videos S1 and S2). Occasional retracting neurites (Figure 3, A–D, tip 4) often exhibited F-tractin accumulations, which moved retrogradely during retraction and gradually disappeared. We were not able to detect elongation of any of the F-tractin–negative neurites, which usually remained completely stationary (Figure 3, A–D, tip 5, and E–H, tip 4).

The amount of data that could be collected using live-cell imaging of F-tractin was limited by a relatively low transfection efficiency of neurons with F-tractin–tdTomato. In addition, expression of F-actin probes can change actin dynamics in cells (Courtemanche *et al.*, 2016). To collect sufficient amount of data for extensive quantification and avoid potential artifacts of F-tractin expression, we performed post hoc phalloidin staining of neurons after imaging them live by time-lapse phase contrast microscopy in the presence of LatB or CytoD (Figure 4). We found that all 141 neurites elongating in the presence of LatB or CytoD without exceptions contained a bright F-actin bulb at their tips (Figure 4E) and exhibited dynamic shape changes (Supplemental Video S3). The elongation rate of neurites undergoing extension in the presence of LatB (0.38 ± 0.25 μm/min [mean ± SD]; 90 neurites) appeared slightly greater than in the presence of CytoD (0.30 ± 0.21 μm/min; 56 neurites, $p = 0.024$) but did not depend on drug concentration. Perhaps a more scattered distribution of remaining F-actin in the presence of CytoD relative to a more focused accumulation of remaining F-actin at neurite tips in the presence of LatB is responsible for the difference in elongation rates. Neurite tips that exhibited dynamic behavior without net outgrowth contained F-actin at the distal tip in majority of cases, whereas only a fraction of immobile and retracting neurites contained F-actin signal at their tips (Figure 4E). Neurites lacking F-actin at the tip never exhibited detectable elongation or shape changes.

Thus, by live-cell imaging, we were unable to detect elongation of neurites that lacked F-actin at their tips, suggesting that neurite outgrowth requires the presence of F-actin. Moreover, constant

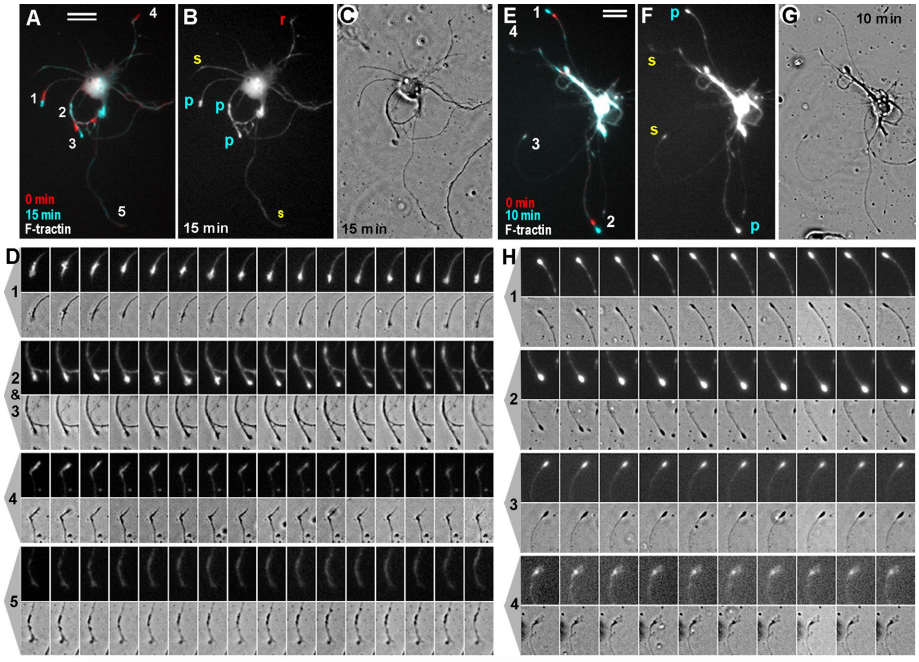

Fraction of F-actin-positive tips				
	Protruding	Dynamic	Stationary	Retracting
LatB (N=12)	100% (n=6)	100% (n=14)	25.0% (n=36)	57.1% (n=7)
CytoD (N=8)	100% (n=13)	100% (n=12)	31.4% (n=35)	100% (n=3)

FIGURE 3: F-actin dynamics in neurons transfected with F-tractin–tdTomato and cultured in the presence of 1 µM LatB (A–D) or 1 µM CytoD (E–H). (A, E) Overlay of F-tractin–tdTomato fluorescence frames taken at time 0 (red) and 15 min (A; cyan) or 10 min (E; cyan). Neurite tips that appear cyan (1–3 in A and 1 and 2 in E) represent actin-rich tips that underwent protrusion; tip 4 in A, which appears red, is an actin-positive tip that underwent retraction; tip 3 in E, which appears white, is a stationary actin-positive tip; faint whitish neurites are actin-negative neurites that remain stationary. (B, F) F-tractin–tdTomato fluorescence frames taken at 15 min (B) or 10 min (F) showing protruding (p), stationary (s), and retracting (r) tips. (C, G) Phase contrast images at 15 min (C) or 10 min (G). (D, H) Enlarged frames from the time-lapse sequence showing fluorescence (top) and phase contrast (bottom) dynamics of the tips numbered in A and E, respectively. Bars, 20 µm. (J) Quantification of neurite behavior in F-tractin–tdTomato expression experiments. *N*, number of transfected cells; *n*, number of neurites. Percentages of F-tractin–positive neurite tips that exhibited indicated behavior in the presence of 1 µM LatB or 1 µM CytoD.

actin-positive tips (Figure 5A, tips 1 and 2) and stationary neurites that either completely lacked F-actin (Figure 5B, tip 4) or had F-actin accumulations away from the neurite tip (Figure 5A, tip 3). EB3 comets were more abundant in relatively thick neurites, likely because such neurites had more microtubules than thin neurites. However, even abundant microtubules repeatedly hitting the plasma membrane of the actin-free neurite tip did not obviously cause membrane protrusion (Figure 5A, tip 3). Conversely, protruding neurites were not necessarily richer in growing microtubules than stationary ones but always contained F-actin signal at their tips (Figure 5A, tip #1). Thus live-imaging data showed that stationary actin-negative neurites contained dynamic microtubules that might drive their outgrowth.

As an additional approach, we used fixed neurons expressing EB3-EGFP only. After treatment of DIV2 neurons with 2.5 µM CytoD for 24 h, cells were fixed and stained with phalloidin and a GFP antibody to better detect the EB3 signal (Figure 5C). The neurites were categorized as actin positive if they contained a distinct F-actin patch at the tip and as EB3 positive if they contained EB3 puncta within the distal 10-µm-long neurite segment. These data showed that only 7.1% of all neurites lacked EB3 puncta (127 neurites from 63 cells), all of which also lacked F-actin at their tips. However, all actin-positive neurites (45.3% of all neurites) and 86.4% of actin-negative neurites (54.7% of all neurites) contained EB3 puncta. These data show that stationary behavior of actin-negative neurites cannot be explained by a lack of microtubule dynamics.

shape changes of F-actin structures at the growing or even stationary neurite tips, together with the fact that they can translocate over distances exceeding their length, support the idea that actin filaments at the tips of drug-treated neurites are dynamic and undergo constant turnover. If they were aggregates of stable unpolymerizable F-actin, it would be hard to explain how they are able change their shape and keep up with the advancing neurite tip.

Actively polymerizing microtubules are present in both actin-positive and actin-negative processes of drug-treated neurons

From the microtubule-centric view of neurite outgrowth, inability of actin-negative neurites to elongate in the presence of actin-depolymerizing drugs could be explained by a lack of microtubule dynamics in these neurites. To test this possibility, we used a microtubule plus end–tracking protein, EB3, to visualize growing microtubule tips in CytoD-treated neurons. Neurons were cotransfected with EB3-mCherry and enhanced green fluorescent protein (EGFP)–LifeAct at DIV1, treated with 2.5 µM CytoD at DIV3, and imaged at DIV4 (Figure 5, A and B, and Supplemental Videos S4 and S5). These data revealed that EB3-positive growing microtubule tips were present in all types of neurites, including protruding and stationary neurites with

Inhibition of microtubules dynamics by Taxol treatment does not stop neurite outgrowth

To functionally test a role of microtubule dynamics for neurite outgrowth in the presence of actin polymerization inhibitors, we stabilized microtubules by treating cells with low concentrations of Taxol and evaluated neurite dynamics. We found that addition of 100 nM Taxol to the culture medium during time-lapse imaging of EB3-mCherry–expressing neurons led to disappearance of moving EB3 comets within 1 min (Supplemental Video S6), indicating quick termination of microtubule growth by Taxol.

We next evaluated whether neurites of CytoD-treated neurons continue to grow in the presence of Taxol. In the first approach, we used neurons expressing an F-actin probe (LifeAct or F-tractin). Cells were pretreated with 1 µM CytoD for ~1 h and then exposed to Taxol. Time-lapse imaging was performed both before and after the addition of Taxol. The results showed that F-actin–positive neurites were able to grow in the presence of Taxol (Figure 6, A and B). Some neurites that were growing before addition of Taxol continued to elongate in the presence of Taxol, whereas other neurites switched their behavior after addition of Taxol from protruding to stationary or from stationary to protruding.

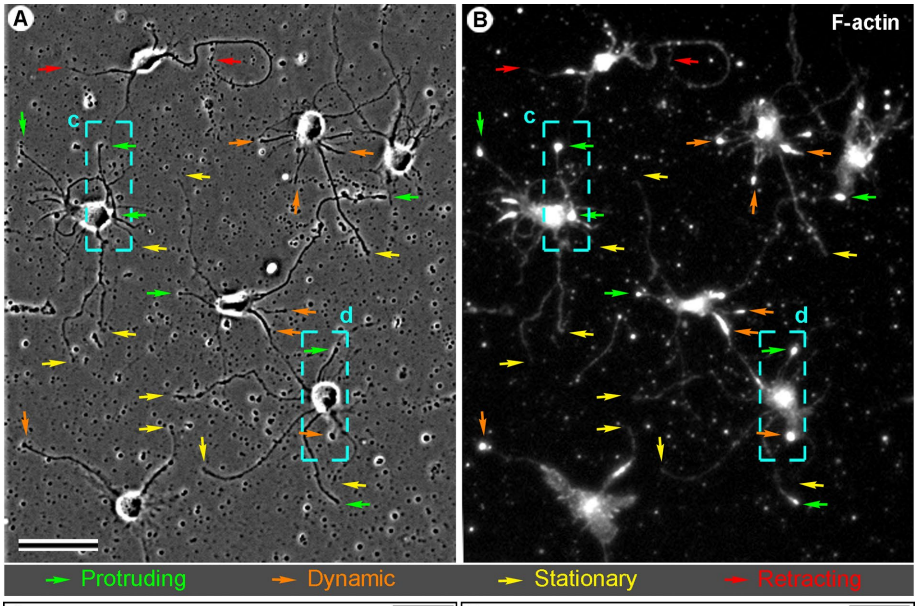

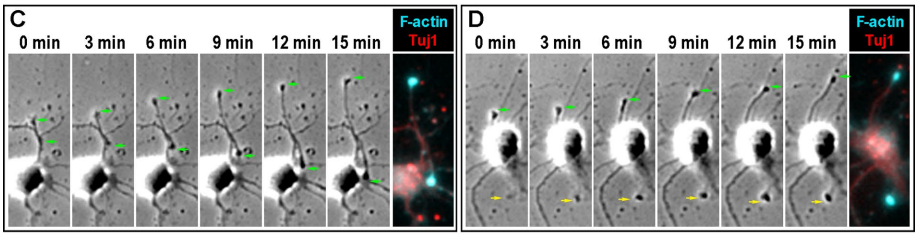

E

FRACTION OF F-ACTIN-POSITIVE TIPS				
	Protruding	Dynamic	Stationary	Retracting
LatB (N=115 cells)	100% (n=94)	97.9 (n=141)	30.0% (n=130)	70.6% (n=17)
CytoD (N=151 cells)	100% (n=47)	94.3% (n=123)	29.8% (n-252)	33.3% (n=9)

FIGURE 4: Post hoc analysis of neurite outgrowth in the presence of LatB and CytoD. (A–D) Neurons treated with 1 μM LatB were recorded by phase contrast time-lapse microscopy for 15 min, fixed, and stained with phalloidin and Tuj1 antibody. (A) Last frame of the phase contrast sequence. (B) The same field as in A after staining with phalloidin. Colored arrows in A and B mark neurite tips that protruded (green), exhibited dynamic behavior without length changes (orange), remained stationary (yellow), or retracted (red) during time-lapse imaging. Bar, 50 μm. (C, D) Frames from the time-lapse sequence for the boxed regions c and d, respectively, labeled in A and B. Green arrows mark tips of elongating neurites. Rightmost images in C and D show post hoc staining of the same regions with phalloidin (cyan) and Tuj1 antibody (red). (E) Quantification of neurite behavior in post hoc experiments after treatment with various concentrations of LatB and CytoD. *N*, number of cells analyzed; *n*, number of neurites. Data show cumulative percentages of F-actin–positive neurite tips for each drug. Concentrations used: 1 μM LatB ($N = 10$; $n = 286$); 2.5 μM LatB ($N = 1$; $n = 11$); 5 μM LatB ($N = 2$, $n = 31$); 10 μM LatB ($N = 3$, $n = 54$); 1 μM CytoD ($N = 14$, $n = 378$); 2 μM CytoD ($N = 1$, $n = 21$), 2.5 μM CytoD ($N = 1$, $n = 5$); 5 μM CytoD ($N = 2$, $n = 21$); and 10 μM CytoD ($N = 1$, $n = 6$).

In the second approach, we applied a post hoc staining strategy. Neurons pretreated with CytoD were imaged by bright-field microscopy before and after addition of Taxol. Then cells were fixed and stained with phalloidin and Tuj1 antibody to correlate protrusive behavior with the presence of F-actin at neurite tips (Figure 6, C and D). Quantification of these results showed that the fraction of protruding neurite tips in cultures pretreated with CytoD for 24 h (7.9 ± 6.5%, 182 neurites from 55 cells in eight movies) was not significantly different from the fraction of protruding neurites in the same samples after application of Taxol (11.6 ± 5.6%, $p = 0.24$). Similar to the observations made by live-cell imaging of LifeAct-expressing neurons, some neurites elongated both before and after addition of Taxol, whereas others changed their behavior. We also performed similar experiments using a shorter (1.5 or 2.5 h) CytoD pretreatment, which resulted in a significantly greater fraction of growing neurites (19.0 ± 10.2%, 271 neurites from 112 cells in 16 movies) compared with the 24-h-long pretreatment ($p = 0.004$) and a greater fraction of F-actin–positive neurite tips (75.1 ± 19.6 vs. 46.7 ± 22.8% in 24-h-treated cultures, $p = 0.01$). Shorter treatment with CytoD led to even less complete inhibition of actin polymerization, which likely translated into more active neurite outgrowth. Of interest, application of Taxol to cultures pretreated with CytoD for 1.5–2.5 h not only failed to inhibit neurite outgrowth but even appeared to stimulate it, because the fraction of protruding neurite tips increased from 19.0 ± 10.2 to 29.3 ± 14.5%, although with a moderate significance level ($p = 0.029$). The neurite outgrowth stimulation by Taxol observed in our experiments is consistent with previous data demonstrating that stabilization of microtubules can stimulate regeneration of axons after injury (Baas and Ahmad, 2013; Ruschel *et al.*, 2015). All elongating neurites, either in the presence of CytoD alone or in the presence of both CytoD and Taxol, contained an F-actin patch at their tips and elongated at indistinguishable rates (0.16 ± 0.1 μm/min; $p = 0.9$; 62 elongating neurites for CytoD only and 96 elongating neurites for CytoD plus Taxol; data from 112 cells in 16 movies). Together these data show that neurites are able to elongate in the absence of growing microtubules but invariably remain stationary or retract if they lack F-actin accumulation at their tips.

Conclusion

The remarkable phenomenon that neurons efficiently extend processes in the presence of actin polymerization inhibitors led to the concept that microtubules in neurons are able to propel plasma membrane at the neurite tip and the actin cytoskeleton is dispensable for this process or even interferes with microtubule access to the plasma membrane. Our data largely rule out this idea by showing that neurites never elongate if they do not have an accumulation of actin filaments at their tips. Existence of these actin filament structures in the presence of inhibitors may seem surprising if one assumes that inhibitors have an absolute power to block actin polymerization. However, basic chemical considerations suggest that inhibition is rarely complete because it involves reversible kinetics of drug–target interaction and therefore depends on affinity between these molecules. Our data show that CytoD and LatB do not fully block actin polymerization, especially at low concentrations or after relatively short treatment. Our data strongly support the idea that this unextinguished actin assembly drives growth cone protrusion in neurons in the presence of low concentrations of inhibitors of actin polymerization, but the ability of neurites to grow declines with

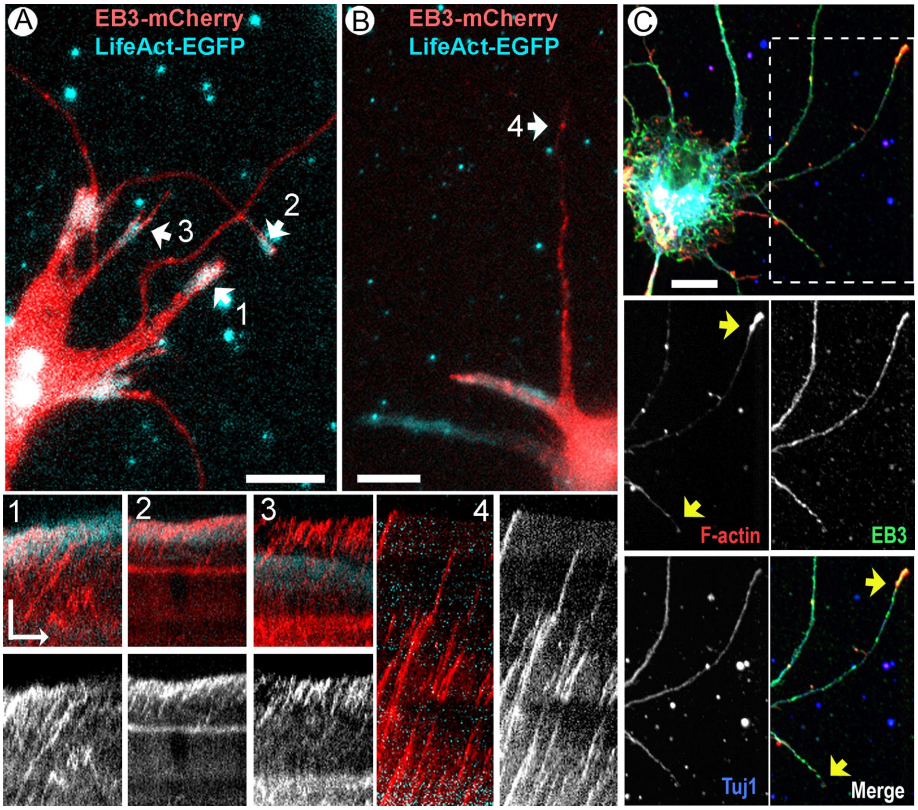

FIGURE 5: Microtubule dynamics in CytoD-treated neurons. (A, B) Snapshots of time-lapse sequences of neurons cotransfected with lentiviral mCherry-EB3 (red) and LifeAct-EGFP constructs (cyan) at DIV1, treated with 2.5 µM CytoD at DIV3 for 24 h, and imaged at DIV4. Numbered arrows indicate neurites shown by kymographs in the bottom images as merged channels and as mCherry-EB3 channel only. Time scale bar, 1 min. Scale bars, 10 µm (snapshots), 5 µm (kymographs). (C) Fluorescence microscopy of EB3-EGFP–expressing DIV3 neurons stained with phalloidin (red) and anti-GFP (green) and Tuj1 (blue) antibodies. Boxed region is zoomed in lower images as individual channels and a merged image. Green EB3 streaks are apparent in both actin-positive and actin-negative neurites.

increasing drug concentration and treatment time. Dynamic behavior of surviving actin structures, their localization at the tips of growing neurites, and branched organization of actin filaments in these structures suggest that neurons use a conventional dendritic nucleation mechanism of actin polymerization to advance the leading tip of neurites. Of interest, we observed neither filopodia nor long actin filaments in drug-treated neurons, suggesting that persistent elongation of actin filaments is not possible in the presence of inhibitors, whereas branched nucleation and short periods of actin elongation are affordable and sufficient for generating protrusion. Together our data support the idea that the classic mechanism of plasma membrane protrusion driven by actin polymerization also functions during neurite extension in the presence of actin polymerization inhibitors. In contrast, microtubule polymerization in neurites lacking actin filaments is not sufficient for neurite extension.

Our findings, however, do not diminish an important role of microtubules in neuron motility but instead redirect attention from the question of how microtubules drive protrusion to how they regulate the actin cytoskeleton that drives protrusion. Research efforts aimed at understanding how microtubules organize cell motility have been ongoing since the original discovery of their role in directional cell migration (Vasiliev *et al.*, 1970) and neurite outgrowth (Yamada *et al.*, 1970). These efforts have resulted in several nonexclusive models, which are constantly undergoing further development (for review, see *Introduction* and Etienne-Manneville, 2013). However, even most advanced models include hypothetical steps carried out by unknown factors. Therefore much work remains to be done to reveal molecular mechanism(s) of actin–microtubule cross-talk. Our findings help to narrow the scope of future studies and thus facilitate progress in this direction.

MATERIALS AND METHODS

Cell culture

Rat hippocampal neurons (obtained from the CNS Cell Culture Service Center at the Mahoney Institute for Neuroscience, University of Pennsylvania School of Medicine, Philadelphia, PA) were isolated and dissected as described previously (Wilcox *et al.*, 1994). Briefly, hippocampi were dissected from the brains of Sprague Dawley rat embryos at embryonic days 18–20 and dissociated into individual cells by incubation in a trypsin-containing solution. The cells were then washed and plated at 60,000–100,000 cells/ml on poly-L-lysine–coated (1 mg/ml) glass coverslips in 35-mm dishes or glass-bottomed 35-mm dishes (Fisher Scientific, Hampton, NH) in 1.5 ml of neurobasal medium (Invitrogen, Carlsbad, CA) with 2% B27 supplement (Invitrogen). LatB (Calbiochem, San Diego, CA) or CytoD (Sigma-Aldrich, St. Louis, MO) was added to cultures 48 h after plating from 1 mM (LatB) or 2 mM (CytoD) stock solutions in DMSO and cultured for an additional 24 h unless stated otherwise.

DNA constructs

F-tractin–tdTomato (amino acids 9–40 from inositol-1,4,5-trisphosphate-3-kinase A fused to tdTomato) was a gift of Michael Schell (Uniformed Services University, Bethesda, MD). To generate F-tractin–mCherry and F-tractin–EGFP in lentiviral expression vectors, F-tractin prototype (amino acids 9–52) was amplified from the F-tractin–pEGFP construct (Johnson and Schell, 2009) using the 5′-GCTCGAATTCATGGGCATGGCG-3′ and 5′-CGGTGGATCCGACCCTGC-3′ primers, digested with *Eco*RI and *Bam*HI, and recloned into pLL-mCherry and pLL-EGFP vectors (gifts from A. Efimov, Fox Chase Cancer Center, Philadelphia, PA), respectively. Similarly, LifeAct (Riedl *et al.*, 2008) was recloned from LifeAct-EGFP (gift from Danijela Vignjevic, Institute Curie, Paris, France) into pLL-mCherry vector after amplification using the 5′-CTTCGAATTCATGGGTGTCGCA-3′ and 5′-CGGTGGATCCCCTTCTTCC-3′ primers and digestion with *Eco*RI and *Bam*HI. pLL-mCherry-EB3 and pLL-EB3-EGFP-constructs were gifts from A. Efimov.

Lentivirus production and infection

HEK293T cells were cultured in DMEM supplemented with 10% fetal bovine serum (FBS) for 24 h before transfection. Cultures at 50–70% confluency were transfected with a mixture of packaging (Pax2), envelope (MD2G), and transfer plasmids using Fugene6 reagent (Promega, Madison, WI). After incubation for 5–6 h with the

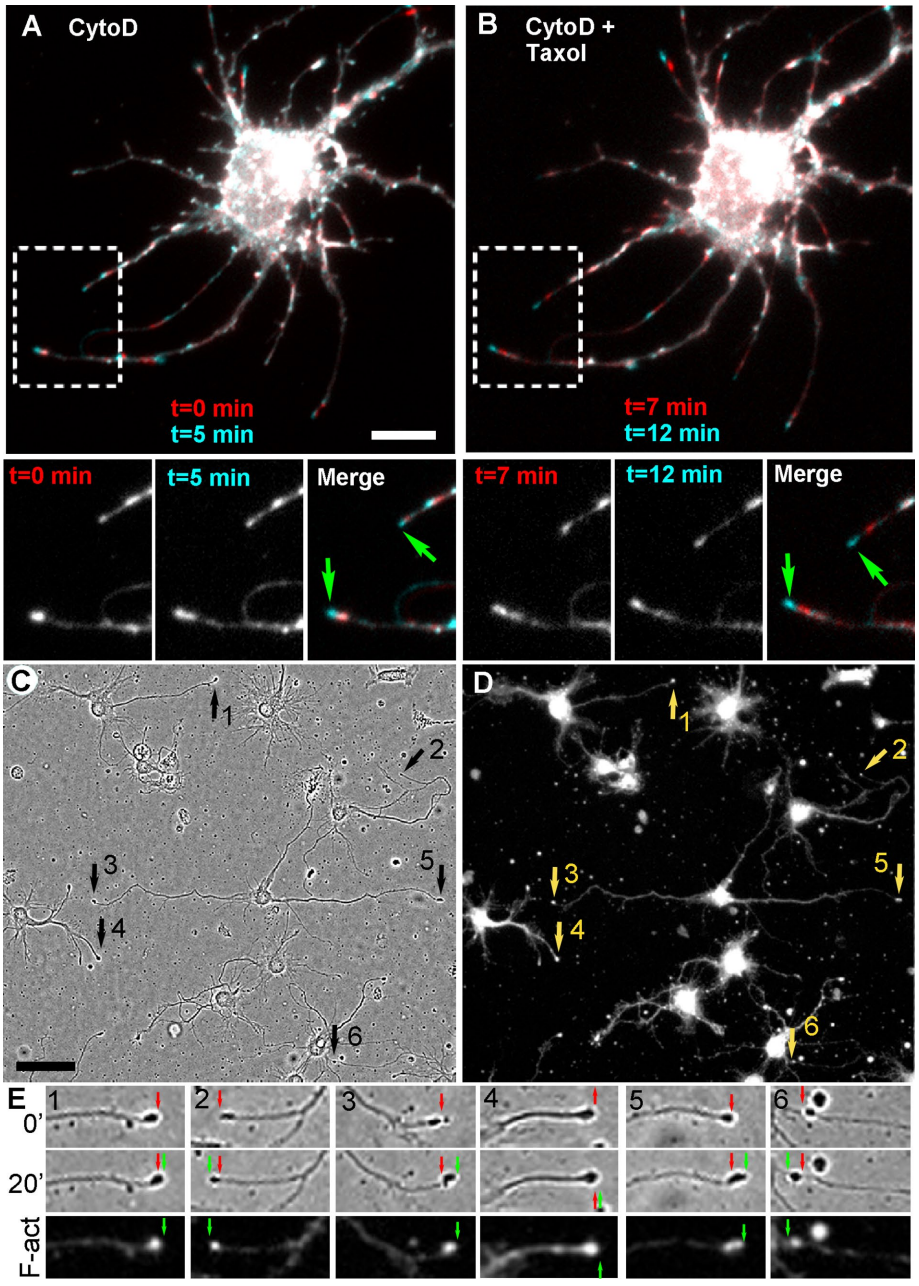

FIGURE 6: Neurite outgrowth in the presence of CytoD and Taxol. (A, B) Neurons expressing mCherry-LifeAct and pretreated with 1 μM CytoD for 1 h. Overlays of two frames (5 min apart) taken in the presence of CytoD only (A) or in the presence of both CytoD and 100 nM Taxol (B). Boxed regions are zoomed in lower images separately and as overlays. Blue tips (green arrows) indicate neurite outgrowth. (C–E) Post hoc analysis of neurite outgrowth in the presence of 1 μM CytoD and 100 nM Taxol. Neurons were pretreated with 1 μM CytoD for 1.5 h, imaged first in the presence of CytoD only and then treated with 100 nM Taxol, recorded by bright-field time-lapse microscopy for 20 min, fixed, and stained with phalloidin and Tuj1 antibody. (C) Last frame of the phase contrast sequence in the presence of Taxol. Numbered arrows mark neurite tips that exhibited extension in the presence of Taxol. (D) The same field as in C after staining with phalloidin. (E) Neurite tips marked by arrows in C are shown at two time points (0 and 20 min) of the bright-field movie and after staining with phalloidin (F-act). Red and green arrows mark initial and final positions of the tips. Bars, 10 μm (A, B), 50 μm (C, D).

transfection mixture, the medium was replaced with DMEM with 10% FBS. The medium containing viral particles was collected 48 h later. Rat hippocampal neurons were infected with lentivirus at DIV1 by incubating them for 5–6 h with virus-containing medium supplemented with 8 μg/ml protamine sulfate (Sigma-Aldrich).

Light microscopy

For fluorescence staining, cells were fixed with 0.2% glutaraldehyde in 0.1 M sodium cacodylate buffer (pH 7.3) either directly or after preextraction with 1% Triton X-100 in PEM buffer (100 mM 1,4-piperazinediethanesulfonic acid–KOH, pH 6.9, 1 mM $MgCl_2$, and 1 mM ethylene glycol tetraacetic acid) containing 2% polyethylene glycol (molecular weight, 35,000), 2 μM phalloidin, and 2 μM Taxol for 3 min at room temperature followed by three rinses with PEM. Fixed samples were quenched twice with 2 mg/ml $NaBH_4$ for 5–10 min, washed in phosphate-buffered saline, and stained with primary mouse monoclonal Tuj1 antibody to neuron-specific tubulin β3 isoform (1:100–1:200 dilution; Covance, Princeton, NJ) and secondary antibody conjugated to Dylight 488 or Dylight 594 (Jackson ImmunoResearch, West Grove, PA) or Alexa Fluor 488, Alexa Fluor 568, or Alexa Fluor 594 (Molecular Probes, Eugene, OR) used at 1:100–1:200 dilution. For actin filament staining, Alexa Fluor 488–, Alexa Fluor 594–, or Alexa Fluor 680–phalloidin (Molecular Probes) was added to secondary antibody solutions at 1:200 dilution.

For live-cell fluorescence imaging of F-actin dynamics (Figure 3), neurons were nucleofected at the time of plating with F-tractin–tdTomato using Neon Transfection system (Invitrogen), cultured for 48 h in glass-bottomed dishes, treated with 1 μM LatB or 1 μM CytoD for 24 h, and imaged by fluorescence and phase contrast microscopy for 15 min at the rate of 1 frame/min in an environmental chamber maintained at 37°C in humidified atmosphere with 5% CO_2. For Figures 5 and 6, neurons were infected at DIV1 with lentivirus carrying pLL-EB3-mCherry, pLL-EB3-EGFP, pLL-LifeAct-mCherry, pLL-F-tractin-mCherry, and/or pLL-F-tractin-EGFP. For post hoc analysis, neurons were cultured in glass-bottomed dishes for 48 h, treated with LatB or CytoD, imaged by phase contrast or bright-field microscopy for 15–20 min, and fixed on the microscope stage with 2% glutaraldehyde by supplying the culture medium with an equivalent volume of 4% glutaraldehyde in Na cacodylate buffer. After staining with phalloidin and Tuj1 antibody, the same regions were found, and fluorescence images of the cells observed in the living state were acquired.

Light microscopy imaging was performed using an Eclipse TE2000-U inverted microscope (Nikon USA, Melville, NY) equipped with Plan Apo 100×/1.3 numerical aperture (NA) and 20×/0.75 NA objectives and a Cascade 512B charge-coupled device (CCD) camera (Photometrics, Tucson, AZ) driven by MetaMorph imaging

software (Molecular Devices, Sunnyvale, CA) or a Nikon Eclipse Ti inverted microscope equipped with CFI60 Apochromat total internal reflection fluorescence 100×/1.49 NA oil and Plain Apo 20×/0.75 NA objectives and a QuantEM 512SC digital camera (Photometrics) driven by NIS-Elements software (Nikon). Channels were combined in different colors after linear contrast adjustment using Photoshop (Adobe Systems, Mountain View, CA). The background of bright-field images was flattened by the Flatten Background tool in MetaMorph. In Supplemental Videos S4 and S5, background was subtracted using a rolling ball radius of 25 pixels, and a median filter of 1 pixel was applied to reduce noise using ImageJ software (National Institutes of Health, Bethesda, MD).

Electron microscopy

Samples for PREM were processed as described previously (Svitkina, 2007, 2009). Briefly, samples were extracted as for light microscopy, sequentially fixed with 2% glutaraldehyde, 0.1% tannic acid, and 0.2% uranyl acetate, critical point dried, coated with platinum and carbon, and transferred onto electron microscopic grids for observation. Samples were examined using a JEM 1011 transmission electron microscope (JEOL USA, Peabody, MA) operated at 100 kV. Images were acquired by an ORIUS 832.10W CCD camera (Gatan, Warrendale, PA) and presented in inverted contrast.

Image analysis and statistics

Measurements were done using ImageJ software. Neurite lengths were measured from the hillock to the tip. Neurite length, number of neurites per cell, and fraction of F-actin-positive tips per cell were determined in three independent experiments using combined phalloidin- and Tuj1-stained images acquired at 20× magnification. Rates of neurite elongation were determined by dividing the total distance traveled by the neurite tip from the beginning to end of the time-lapse sequence by the duration of the sequence. Statistical analysis (analysis of variance) was performed using Instat (GraphPad, San Diego, CA) software. Significance was determined using Kruskal–Wallis and Dunn's multiple comparisons tests. Graphs were produced using Excel software (Microsoft, Redmond, CA).

ACKNOWLEDGMENTS

We thank A. Efimov and D. Vignjevic for generous gifts of reagents. This work is supported by National Institutes of Health Grant GM-095977.

REFERENCES

Andrianantoandro E, Blanchoin L, Sept D, McCammon JA, Pollard TD (2001). Kinetic mechanism of end-to-end annealing of actin filaments. J Mol Biol 312, 721–730.

Baas PW, Ahmad FJ (2013). Beyond taxol: microtubule-based treatment of disease and injury of the nervous system. Brain 136, 2937–2951.

Banker GA, Cowan WM (1977). Rat hippocampal neurons in dispersed cell culture. Brain Res 126, 397–342.

Bonder EM, Mooseker MS (1986). Cytochalasin B slows but does not prevent monomer addition at the barbed end of the actin filament. J Cell Biol 102, 282–288.

Bradke F, Dotti CG (1999). The role of local actin instability in axon formation. Science 283, 1931–1934.

Bradke F, Fawcett JW, Spira ME (2012). Assembly of a new growth cone after axotomy: the precursor to axon regeneration. Nat Rev Neurosci 13, 183–193.

Bridgman PC, Kachar B, Reese TS (1986). The structure of cytoplasm in directly frozen cultured cells. II. Cytoplasmic domains associated with organelle movements. J Cell Biol 102, 1510–1521.

Buck KB, Zheng JQ (2002). Growth cone turning induced by direct local modification of microtubule dynamics. J Neurosci 22, 9358–9367.

Collins A, Warrington A, Taylor KA, Svitkina T (2011). Structural organization of the actin cytoskeleton at sites of clathrin-mediated endocytosis. Curr Biol 21, 1167–1175.

Courtemanche N, Pollard TD, Chen Q (2016). Avoiding artefacts when counting polymerized actin in live cells with LifeAct fused to fluorescent proteins. Nat Cell Biol 18, 676–683.

Dent EW, Gupton SL, Gertler FB (2011). The growth cone cytoskeleton in axon outgrowth and guidance. Cold Spring Harb Perspect Biol 3, a001800.

Dent EW, Kalil K (2001). Axon branching requires interactions between dynamic microtubules and actin filaments. J Neurosci 21, 9757–9769.

Etienne-Manneville S (2013). Microtubules in cell migration. Annu Rev Cell Dev Biol 29, 471–499.

Flynn KC, Hellal F, Neukirchen D, Jacob S, Tahirovic S, Dupraz S, Stern S, Garvalov BK, Gurniak C, Shaw AE, *et al.* (2012). ADF/Cofilin-mediated actin retrograde flow directs neurite formation in the developing brain. Neuron 76, 1091–1107.

Forscher P, Smith SJ (1988). Actions of cytochalasins on the organization of actin filaments and microtubules in a neuronal growth cone. J Cell Biol 107, 1505–1516.

Gallo G (2013). Mechanisms underlying the initiation and dynamics of neuronal filopodia: from neurite formation to synaptogenesis. Int Rev Cell Mol Biol 301, 95–156.

Gundersen GG, Bulinski JC (1988). Selective stabilization of microtubules oriented toward the direction of cell migration. Proc Natl Acad Sci USA 85, 5946–5950.

Johnson HW, Schell MJ (2009). Neuronal IP3 3-kinase is an F-actin-bundling protein: role in dendritic targeting and regulation of spine morphology. Mol Biol Cell 20, 5166–5180.

Kaverina I, Krylyshkina O, Small JV (2002). Regulation of substrate adhesion dynamics during cell motility. Int J Biochem Cell Biol 34, 746–761.

Korobova F, Svitkina T (2008). Arp2/3 complex is important for filopodia formation, growth cone motility, and neuritogenesis in neuronal cells. Mol Biol Cell 19, 1561–1574.

Krendel M, Zenke FT, Bokoch GM (2002). Nucleotide exchange factor GEF-H1 mediates cross-talk between microtubules and the actin cytoskeleton. Nat Cell Biol 4, 294–301.

Letourneau PC, Shattuck TA, Ressler AH (1987). "Pull" and "push" in neurite elongation: observations on the effects of different concentrations of cytochalasin B and taxol. Cell Motil Cytoskeleton 8, 193–209.

Lu W, Fox P, Lakonishok M, Davidson MW, Gelfand VI (2013). Initial neurite outgrowth in Drosophila neurons is driven by kinesin-powered microtubule sliding. Curr Biol 23, 1018–1023.

Mullins RD, Heuser JA, Pollard TD (1998). The interaction of Arp2/3 complex with actin: nucleation, high affinity pointed end capping, and formation of branching networks of filaments. Proc Natl Acad Sci USA 95, 6181–6186.

Paluch EK, Raz E (2013). The role and regulation of blebs in cell migration. Curr Opin Cell Biol 25, 582–590.

Rajnicek AM, Foubister LE, McCaig CD (2006). Growth cone steering by a physiological electric field requires dynamic microtubules, microfilaments and Rac-mediated filopodial asymmetry. J Cell Sci 119, 1736–1745.

Riedl J, Crevenna AH, Kessenbrock K, Yu JH, Neukirchen D, Bista M, Bradke F, Jenne D, Holak TA, Werb Z, *et al.* (2008). Lifeact: a versatile marker to visualize F-actin. Nat Methods 5, 605–607.

Ruschel J, Hellal F, Flynn KC, Dupraz S, Elliott DA, Tedeschi A, Bates M, Sliwinski C, Brook G, Dobrindt K, *et al.* (2015). Axonal regeneration. Systemic administration of epothilone B promotes axon regeneration after spinal cord injury. Science 348, 347–352.

Ruthel G, Hollenbeck PJ (2000). Growth cones are not required for initial establishment of polarity or differential axon branch growth in cultured hippocampal neurons. J Neurosci 20, 2266–2274.

Siegrist SE, Doe CQ (2007). Microtubule-induced cortical cell polarity. Genes Dev 21, 483–496.

Svitkina T (2007). Electron microscopic analysis of the leading edge in migrating cells. Methods Cell Biol 79, 295–319.

Svitkina T (2009). Imaging cytoskeleton components by electron microscopy. Methods Mol Biol 586, 187–206.

Svitkina TM (2013). Ultrastructure of protrusive actin filament arrays. Curr Opin Cell Biol 25, 574–581.

Svitkina TM, Borisy GG (1999). Arp2/3 complex and actin depolymerizing factor/cofilin in dendritic organization and treadmilling of actin filament array in lamellipodia. J Cell Biol 145, 1009–1026.

Svitkina TM, Verkhovsky AB, McQuade KM, Borisy GG (1997). Analysis of the actin-myosin II system in fish epidermal keratocytes: mechanism of cell body translocation. J Cell Biol 139, 397–415.
Tanaka E, Ho T, Kirschner MW (1995). The role of microtubule dynamics in growth cone motility and axonal growth. J Cell Biol 128, 139–155.
Vasiliev JM, Gelfand IM, Domnina LV, Ivanova OY, Komm SG, Olshevskaja LV (1970). Effect of colcemid on the locomotory behaviour of fibroblasts. J Embryol Exp Morphol 24, 625–640.
Waterman-Storer CM, Worthylake RA, Liu BP, Burridge K, Salmon ED (1999). Microtubule growth activates Rac1 to promote lamellipodial protrusion in fibroblasts. Nat Cell Biol 1, 45–50.
Wilcox KS, Buchhalter J, Dichter MA (1994). Properties of inhibitory and excitatory synapses between hippocampal neurons in very low density cultures. Synapse 18, 128–151.
Witte H, Neukirchen D, Bradke F (2008). Microtubule stabilization specifies initial neuronal polarization. J Cell Biol 180, 619–632.
Yamada KM, Spooner BS, Wessells NK (1970). Axon growth: roles of microfilaments and microtubules. Proc Natl Acad Sci USA 66, 1206–1212.
Zhang Y, Zhang XF, Fleming MR, Amiri A, El-Hassar L, Surguchev AA, Hyland C, Jenkins DP, Desai R, Brown MR, *et al*. (2016). Kv3.3 channels bind Hax-1 and Arp2/3 to assemble a stable local actin network that regulates channel gating. Cell 165, 434–448.